Dual-Focus Fluorescence Correlation Spectroscopy of Colloidal Solutions: Influence of Particle Size

Claus B. Müller,[†] Anastasia Loman,[‡] Walter Richtering,[†,*] and Jörg Enderlein[‡,*]

Institute of Physical Chemistry, RWTH Aachen University, Landoltweg 2, 52056 Aachen, Germany, and Institute of Physical and Theoretical Chemistry, Eberhard Karls University, Auf der Morgenstelle 8, 72076 Tübingen, Germany

Received: March 16, 2008; Revised Manuscript Received: April 28, 2008

Fluorescence correlation spectroscopy (FCS) is a powerful technique for measuring diffusion coefficients of small fluorescent molecules at pico- to nanomolar concentrations. Recently, a modified version of FCS, dual-focus FCS (2fFCS), was introduced that significantly improves the reliability and accuracy of FCS measurements and allows for obtaining absolute values of diffusion coefficients without the need of referencing again a known standard. It was shown that 2fFCS gives excellent results for measuring the diffusion of small molecules. However, when measuring colloids or macromolecules, the size of these objects can no longer be neglected with respect to the excitation laser focus. Here, we analyze how 2fFCS data evaluation has to be modified for correctly taking into a count these finite size effects. We exemplify the new method of measuring the absolute size of polymeric particles with simple and complex fluorophore distributions.

Introduction

Thermally induced Brownian motion of molecules and particles in solution is a fundamental property that is macroscopically described by the diffusion coefficient. The famous Stokes−Einstein equation[1] relates the diffusion coefficient of spherical objects to their hydrodynamic radius R_h, which is, for molecules, a measure of their size including interaction effects with the surrounding solvent (e.g., hydration shell). Standard methods for measuring diffusion coefficients are dynamic light scattering (DLS),[2] pulsed field gradient nuclear magnetic resonance (pfgNMR),[3] or analytical ultracentrifugation.[4] These methods can measure diffusion coefficients with an accuracy of better than a few percent. However, they need either large particle size and/or large concentrations for yielding sufficient signal intensity to make diffusion measurements feasible. In contrast, fluorescence correlation spectroscopy (FCS), which was developed in the early 1970s by Elson, Magde, and Webb,[5–7] determines diffusion coefficients at pico- to nanomolar concentrations by measuring fluorescence fluctuations out of a very small detection volume, typical on the range of a femtoliter. Also FCS has found manifold applications in many areas of research; the quantitative outcome of an FCS measurement depends on many particularities of the optical setup and the photophysics of the used fluorophores, making precise measurements rather difficult. Moreover, because standard FCS measurements lack an external length scale, one has, for obtaining absolute values of a diffusion coefficient, to reference each measurement against a standard of known diffusion.

Recently, a modified version of FCS, so-called dual-focus FCS or 2fFCS,[8] was introduced, allowing absolute and precise diffusion measurements, without suffering from the pitfalls of standard FCS. The method was shown to yield exact values for diffusion coefficients of fluorescent dyes with an accuracy better than 5%. The core idea was to generate two overlapping foci with known distance and to measure and evaluate the autocorrelation function of each focus as well as the cross-correlation function between the foci. However, until now the method was only applied to small molecules that could be considered pointlike with respect to the size of the detection region, which simplifies the analysis significantly.

For employing 2fFCS for diffusion measurements of extended objects with complex fluorophore distribution, their size and fluorophore distribution in comparison with the size of detection volume has to be taken into account. Because 2fFCS is a very precise method, fitting correlation curves that were measured on extended objects but using the assumption of pointlike particles lead to an unsatisfactory fit quality. For measuring extended objects with single focus FCS, Starchev et al.[9] proposed the idea of increasing the effective detection volume with object size. For the precision of 2fFCS, this model is not able to describe sufficiently the obtained autocorrelation function (ACF).

Here, we modify the data analysis of 2fFCS to take into account the finite size of diffusing particles, allowing for an arbitrary but spherically symmetric fluorophore distribution within the particle. The resulting modification is applied to analyzing 2fFCS on dye-doped latex particles with different internal fluorophore distribution. We show that the method yields results for particle size with nanometer accuracy. Thus, 2fFCS may be an important complimentary measurement technique for studies in colloid and polymer science[10–17] or for studying molecular aggregation.

Materials and Setup

TetraSpeck fluorescent microsphere standards (0.1 μm, T7279; 0.2 μm, T7280; 0.5 μm, T7281; and 1.0 μm, T7282) were purchased from Invitrogen (Karlsruhe, Germany). As standard solvent, LichroSolv water for chromatography (No. 115333) was purchased from Merck (Darmstadt, Germany). TetraSpeck latex particles consist of continuously fluorescent

* Corresponding authors. E-mail: richtering@pc.rwth-aachen.de (W.R.), joerg.enderlein@uni-tuebingen.de (J.E.).
[†] RWTH Aachen University.
[‡] Eberhard Karls University.

10.1021/jp802280u CCC: $40.75
Published on Web 06/21/2008

labeled spherical beads, by specification of the manufacturer. The beads contain a mixture of four fluorescent dyes with well-separated excitation/emission peaks (365/430 nm, 505/515 nm, 560/580 nm, and 660/680 nm).

The 2fFCS setup is based on a MicroTime200 inverse time-resolved fluorescence microscope (MT200, PicoQuant, Berlin, Germany) as described in ref 18. The dual-focus extension of the setup was described in ref 8. In short, two identical pulsed laser beams at 635 nm wavelength (LDH-P-635, PicoQuant, Berlin, Germany) each orthogonal to the other's linear polarization are combined by a polarizing beam splitter into a single light beam. After spatial filtering to obtain a perfect Gaussian profile, the excitation light is coupled into the excitation path of the microscope. Before entering the microscope's objective, the light is passed though a Nomarski prism, as used in standard differential interference contrast (DIC) microscopy. The prism deflects the light according to polarization, so that the light from the first laser is slightly deflected to one side and the light of the second laser to the other. Thus, after focusing through a water immersion objective (UPLAPO 60 × W, 1.2 N.A., Olympus Europa, Hamburg, Germany), two overlapping foci with a small lateral shift are generated within the sample solution. The distance between them was determined as described in ref 19. Fluorescence is collected by the same objective, passed through filters blocking any laser backscatter, and subsequently focused onto a confocal aperture of 200 μm diameter. After recollimation, the fluorescence light is split by a nonpolarizing beam splitter and refocused for detection on two single-photon avalanche diodes (SPAD, PDM series, detector diameter 50 μm, Micro Photon Devices, Bolzano, Italy). A dedicated single photon counting electronics (PicoHarp 300, PicoQuant, Berlin, Germany) is used for recording photon detection events in time tagged time-resolved (TTTR) mode[18] with a temporal resolution of 4 ps. The TTTR mode allows for subsequent calculation of fluorescence decay curves (as in time-correlated single-photon counting or TCSPC[20]) and fluorescence correlation curves. For the latter, a custom written routine able to process asynchronous single photon data is used[21] and only photons from different SPADs are correlated for preventing that SPAD after pulsing effects the resulting correlation functions.

As already mentioned, excitation is done by two pulsed lasers. The laser pulse width is equal to 50 ps. For 2fFCS, the lasers are pulsed alternately[22] for so-called pulsed-interleaved excitation (PIE)[22,23] with an overall repetition rate of 40 or 20 MHz (depending on the fluorescence lifetime of the used fluorophores), using special laser driver electronics (PDL 828, Sepia-II, PicoQuant, Berlin, Germany).

PIE, in conjunction with recording photon detection events with picosecond temporal resolution, allows an unequivocal identification by which laser and thus in which focal volume a photon was generated: any photon arriving within 12.5 ns (or 25 ns for 20 MHz overall repetition rate) after the last laser pulse is attributed to the last pulsing laser. The chance of erroneously attributing a photon to the wrong laser is negligible, because the fluorescence lifetime of the dye was determined as 4.1 ns and is therefore much shorter than the assigned detection time gate.

During measurements, sample temperature was controlled by a custom-made temperature control.[24] The absolute accuracy of temperature control in the focal volume was ±0.1 K. Samples were sealed into sample cells to prevent solvent evaporation. For long-time measurements, the microscope is equipped with an automatic immersion water supply.

Theory

Size Effects. In this subsection, we consider the impact of the non-negligible size of an object on its fluorescence ACF. Let us assume that the distribution of fluorescent dye within the object is spherically symmetric and described by the function $\upsilon(r)$, $0 \le r \le a$. Then, the lag-time-dependent part of the ACF is given by the multiple integral

$$g(t) \sim \int \mathrm{d}\mathbf{u}_2 \int \mathrm{d}\mathbf{r}_2 \int \mathrm{d}\mathbf{r}_1 \int \mathrm{d}\mathbf{u}_1\, \upsilon(u_2)\, U(\mathbf{r}_2 + \mathbf{u}_2)\, G(\mathbf{r}_2 - \mathbf{r}_1, t)\, U(\mathbf{r}_1 + \mathbf{u}_1)\, \upsilon(u_1) \quad (1)$$

where $U(\mathbf{r})$ is the molecule detection function (MDF), which is proportional to the probability of detecting a fluorescence photon from a molecule at position $\mathbf{r}$, and $G(\mathbf{r}_2-\mathbf{r}_1,t)$ is the probability density that the object's center has moved from $\mathbf{r}_1$ to $\mathbf{r}_2$within time interval t,

$$G(\mathbf{r}, t) = \frac{1}{(4\pi D t)^{3/2}} \exp\left(-\frac{|\mathbf{r}|^2}{4Dt}\right) \quad (2)$$

which is nothing else then Green's function[25] of the free diffusion equation. Thus, the ACF for an extended object is similar to the ACF of a pointlike particle when moving within a measurement system with the modified MDF

$$\bar{U}(\mathbf{r}) = \int \mathrm{d}\mathbf{u}\, \upsilon(u)\, U(\mathbf{r} + \mathbf{u}) = \int \mathrm{d}\mathbf{r}'\, \upsilon(|\mathbf{r} - \mathbf{r}'|)\, U(\mathbf{r}') \quad (3)$$

There is an efficient way to calculate the modified MDF $\bar{U}(\mathbf{r})$. For the sake of simplicity, let us assume that the MDF $U(\mathbf{r})$ is rotationally symmetric around the optical axis [i.e., $U(\mathbf{r}) = U(\rho,z)$ in cylindrical coordinates with z along the optical axis] and mirror symmetric with respect to the plane $z = 0$. In that case, one can represent $U(\mathbf{r})$ by an expansion into Fourier and Bessel components of the form

$$U(\mathbf{r}) \equiv U(\rho, z) = \int_{-\infty}^{\infty} \frac{\mathrm{d}q}{2\pi} \int_0^{\infty} \mathrm{d}k\, k\tilde{U}(k, q)\, J_0(k\rho) \cos(qz) \quad (4)$$

A detailed derivation and explanation of the Fourier and Bessel integral theorem can be found in ref 26. Next, one rewrites the fluorophore distribution function $\upsilon(\mathbf{r}) = \upsilon(|\mathbf{r}|) = \upsilon(\sqrt{(\rho^2 + z^2)})$ into a similar expansion:

$$\upsilon(|\mathbf{r}|) = \int_{-\infty}^{\infty} \frac{\mathrm{d}q}{2\pi} \int_0^{\infty} \mathrm{d}k\, k\tilde{\upsilon}(k, q)\, J_0(k\rho) \cos(qz) \quad (5)$$

Using the well-known addition theorem for Bessel functions[26] (translation along x-axis by r_0)

$$J_0(kR) = \sum_{m=-\infty}^{\infty} J_m(kr_0)\, J_m(kr) \mathrm{e}^{\mathrm{i}m\varphi} \quad (6)$$

one finds

$$\upsilon(|\mathbf{r} - \mathbf{r}'|) = \int_{-\infty}^{\infty} \frac{\mathrm{d}q}{2\pi} \int_0^{\infty} \mathrm{d}k\, k\tilde{\upsilon}(k, q) \sum_{m=-\infty}^{\infty} J_m(k'\rho)\, J_m(k\rho) \mathrm{e}^{\mathrm{i}q(z-z')+\mathrm{i}m(\varphi-\varphi')} \quad (7)$$

for the function υ shifted to a new origin at $r' = (\rho',\phi',z')$. Inserting these expressions into the integral of $\bar{U}(\mathbf{r})$ and using the closure relation

$$\int_0^\infty \mathrm{d}\rho\, \rho J_0(k'\rho)\, J_0(k\rho) = \frac{1}{k}\delta(k-k') \tag{8}$$

one finally finds

$$\overline{U}(\rho, z) = \int_0^\infty \mathrm{d}q \int_0^\infty \mathrm{d}k\, k\tilde{v}(k,q)\, \widetilde{U}(k,q)\, J_0(k\rho)\mathrm{e}^{\mathrm{i}qz} \tag{9}$$

where the expansion coefficients are given by

$$\widetilde{U}(k,q) = \int_{-\infty}^\infty \mathrm{d}z \int_0^\infty \mathrm{d}\rho\, \rho U(\rho, z)\, J_0(k\rho)\mathrm{e}^{-\mathrm{i}qz} \tag{10}$$

and similarly for $\tilde{v}(k,q)$. Finally, representing Green's function in eq 2 also by its transform

$$G(\mathbf{r}, t) = \int \frac{\mathrm{d}^3\mathbf{k}}{(2\pi)^3} \exp(\mathrm{i}\mathbf{k}\cdot\mathbf{r} - Dk^2 t) \tag{11}$$

and inserting eqs 3, 9, and 11 into eq 1 led to the following compact expression for the time-dependent part of the ACF:

$$g(t) = \varepsilon^2 \int \mathrm{d}k\, k \int \mathrm{d}q \exp[-D(k^2+q^2)t] |\overline{\widetilde{U}}(k,q)|^2 \tag{12}$$

Here, the transform $\bar{\tilde{U}}(k,q)$ is simply the product of $\tilde{U}(k,q)$ with $\tilde{v}(k,q)$, and ε is a constant taking into account the overall excitation and detection efficiency as well as the concentration of particles. It is important to mention that expression 12 is valid also for point-sized particles (or molecules) if one replaces the modified function $\bar{U}(\mathbf{r})$ by the original MDF $U(\mathbf{r})$. Thus, the influence of any size effect on the ACF is completely absorbed by the modified function $\bar{U}(\mathbf{r})$ or $\bar{\tilde{U}}(k,q)$, respectively.

In the present paper, we will consider three types of fluorophore distribution $v(r)$: (i) uniform distribution throughout the particle, (ii) uniform distribution within an outer shell (i.e., particles with nonfluorescent core), and (iii) uniform distribution only within the core of a particle (i.e., particles with nonfluorescent shell).

2fFCS Data Evaluation. The general theoretical background 2fFCS data evaluation was explained in detail in ref 8. Here, we present only a brief introduction into the subject. As already explained in the previous section, 2fFCS uses a Nomarski prism and two identical but orthogonally polarized laser beams for generating two overlapping, laterally shifted foci. Using pulsed interleaved excitation and TCSPC signal recording, one can distinguish in which focus a photon was generated, thus allowing calculation of separate ACFs for each focus but also the cross-correlation function (CCF) between foci, i.e., the probability to detect two photons from the two different foci with a given lag time between them. For extended objects, the ACF can be calculated as discussed in the previous section, see eq 1. For the CCF, a similar expression exists,

$$g_{\mathrm{CCF}}(t) = \varepsilon_1\varepsilon_2 \int \mathrm{d}\mathbf{u}_2 \int \mathrm{d}\mathbf{r}_2 \int \mathrm{d}\mathbf{r}_1 \int \mathrm{d}\mathbf{u}_1\, v(u_2)\, U(\mathbf{r}_2+\mathbf{u}_2)\, G(\mathbf{r}_2-\mathbf{r}_1-\boldsymbol{\delta}, t)\, U(\mathbf{r}_1+\mathbf{u}_1)\, v(u_1) \tag{13}$$

where one has now the additional vector $\boldsymbol{\delta}$ connecting the center positions of both foci, and ε_1 and ε_2 refer now to the first and second focus, respectively. Repeating the same line of reasoning as in the last section, this leads to a similar expression as eq 12,

$$g_{\mathrm{CCF}}(t) \sim \int \mathrm{d}k\, k \int \mathrm{d}q \exp[-D(k^2+q^2)t] J_0(k\delta) |\overline{\widetilde{U}}(k,q)|^2 \tag{14}$$

where the additional zero-order Bessel function $J_0(k\delta)$ appears.

As was shown by Enderlein et al.,[8] an excellent approximation of the MDF $U(\mathbf{r})$ is given by

$$U(\mathbf{r}) = \frac{\kappa(z)}{w^2(z)} \exp\left[-\frac{2}{w^2(z)}(x^2+y^2)\right] \tag{15}$$

where $w(z)$ and $\kappa(z)$ are two functions given by

$$w(z) = w_0\left[1 + \left[\frac{\lambda_{\mathrm{ex}} z}{\pi {w_0}^2 n}\right]^2\right]^{1/2} \tag{16}$$

and

$$k(z) = 2\int_0^a \frac{d\rho\, \rho}{R^2(z)} \exp\left(-\frac{2\rho^2}{R^2(z)}\right) = 1 - \exp\left[-\frac{2a^2}{R^2(z)}\right] \tag{17}$$

where the function $R(z)$ is defined by an expression similar to eq 5:

$$R(z) = R_0\left[1 + \left[\frac{\lambda_{\mathrm{em}} z}{\pi {R_0}^2 n}\right]^2\right]^{1/2} \tag{18}$$

In the above equations, λ_{ex} is the excitation wavelength, λ_{em} is the center emission wavelength, n is the refractive index of the immersion medium (water), a is the radius of the confocal aperture divided by magnification, and w_0 and R_0 are two (generally unknown) model parameters describing the minimum beam waist of one focus and image size of a point emitter in image plane (confocal aperture plane), respectively.

For calculating the ACF and CCF, one uses eqs 15–18 together with eq 10 to compute $\tilde{U}(k,q)$ and then uses eqs 12 and 14 for calculating the correlation functions. Fitting of experimental data is done globally for both ACFs and CCF, where one has the free fit parameters ε_1, ε_2, w_0, R_0, and D.

Results and Discussion

First, a theoretical estimation was made of the influence of the finite size of the diffusing particles on an ACF. We calculated ACFs using typical experimental parameters (w_0 = 500 nm, R_0 = 200 nm, pinhole radius a_0 = 200 μm, magnification 60×, excitation wavelength λ_{ex} = 637 nm, emission wavelength λ_{em} = 670 nm, temperature 298.15 K, viscosity of water η = 0.890 mPa s, refractive index of water n = 1.332) and for different radius values and label distributions.

Computed ACFs for center and uniformly labeled particles with R_{h} = 100 nm and R_{h} = 500 nm are presented in Figure 1. For 100 nm particles ($R_{\mathrm{h}} \ll w_0$), the difference between center-labeled, uniformly labeled, and shell-labeled particles is negligible. However, for 500 nm particles ($R_{\mathrm{h}} \sim w_0$), the size of the particles starts to show up in a shift of the ACF of the uniformly labeled particles to longer times, as compared with the center-labeled particles. For shell-labeled particles, the shifting of the ACF is even more pronounced and allows distinguishing between differently labeled particles. Moreover, the ratio of ACF to CCF amplitude is the smallest for shell-labeled particles. Especially this latter fact is important for a quantitative data analysis: In a standard FCS experiment, the shift of the ACF to longer times could be misinterpreted as the result of a smaller diffusion coefficient of a pointlike particle, but in 2fFCS data evaluation, the changing amplitude ratio hints to a nonpointlike label distribution.

For further elucidating the impact of size and fluorophore distribution, we calculated R_{h} (using the same parameter set as mentioned above) for different apparent diffusion times (inflection point of ACF or CCF, respectively). Several realistic situations are shown in Figure 2: (i) center labeling (one

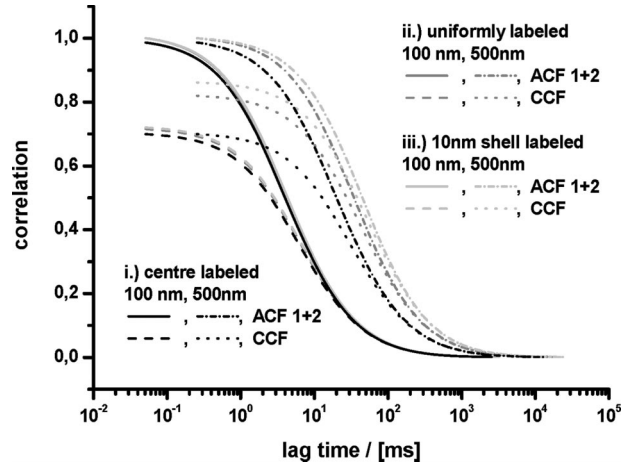

Figure 1. Autocorrelation function of particles with a hydrodynamic radius of 100 nm (red + black) and 500 nm (green + blue), label grade: (i) center labeling, (ii) homogenously distributed labeling of whole particle, (iii) homogenously distributed labeling in 10 nm shell. Parameter set: beam waist $w_0 = 500$ nm, pinhole parameter $R_0 = 200$ nm, pinhole radius $a_0 = 200$ μm, excitation wavelength $\lambda_{ex} = 637$ nm, emission wavelength $\lambda_{em} = 670$ nm, temperature 298.15 K, viscosity of water $\eta = 0.890$ mPa s, refractive index of water $n = 1.332$.

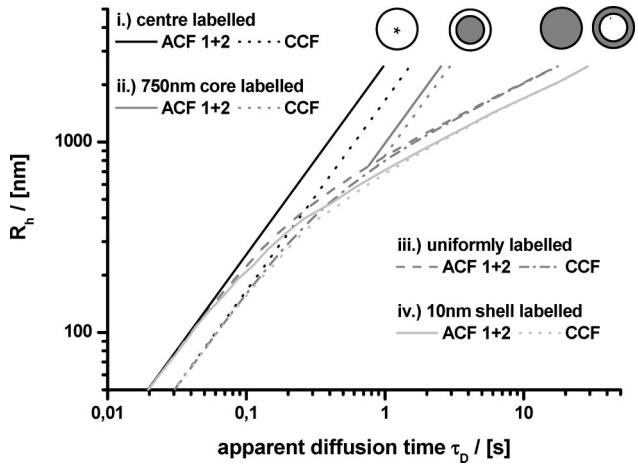

Figure 2. Hydrodynamic radius (R_h) as function of diffusion time: Comparison between particles with only one fluorescent dye, homogenously distributed dyes in whole particle, particles with fluorescent shell of 10 nm thickness, and with a fluorescent core of 750 nm radius (used parameter set as in Figure 1).

fluorophore at the particle's center), (ii) labeling a fixed core radius of 750 nm with varying unlabeled shell thickness, (iii) uniform labeling of the whole particle, and (iv) labeling of a shell of 10 nm thickness and unlabeled core.

The curves are calculated for total particle radius values in the range between $R_h = 50$ and 2500 nm, except for case ii, where the minimum radius is 750 nm. The considered cases can be divided into two groups. For the first group (i and ii), the fluorescently labeled region does not change its size when the total particle radius R_h increases, whereas for the second group (iii and iv), the size of the labeled region increases together with increasing particle radius.

As expected, for all cases of extended labeling, the apparent diffusion time is larger than for an equally sized particle with center labeling. Remarkably, different label distributions lead to distinctly different changes of ACF and CCF diffusion time, which could be used to distinguish between different labeling geometries. Comparing core labeling (case ii) with center labeling (case i), the resulting ACF and CCF are shifted toward longer apparent diffusion times, and the ratio of ACF to CCF amplitude is getting slightly smaller. In contrast, uniform and shell labeling show a much stronger shift of apparent diffusion time and a tremendous decrease in amplitude ratio. When analyzing only the ACF (as done in standard single-focus FCS), the extra shift of the apparent diffusion time (as compared to center labeling) could be easily misinterpreted as larger particle size and could introduce an error in size estimation of several orders of magnitude, as can be seen in Figure 2.

TABLE 1: Hydrodynamic Radius (R_h) of Latex Particles: Specified Radius from Manufacturer Compared with Determined Radius from DLS Experiments

	R_h/nm	
sample	specified	DLS
TS 100	50 ± 3	55.6 ± 0.6
TS 200	105 ± 11	101.5 ± 0.7
TS 500	250 ± 10	255.6 ± 2.3
TS 1000	500 ± 16	488.9 ± 5.5

Second, for experimentally checking the applicability of our modified data analysis, we performed DLS and 2fFCS measurements on uniformly labeled latex beads. The used TetraSpeck latex beads are available with various diameters and can serve as ideal model systems of uniformly labeled spherical particles. DLS measurements were performed on a standard ALV 5000 system, equipped with an excitation laser with 633 nm wavelength. Scattering intensity were detected at scattering angles of 60°, 90°, and 120°. R_h of the particles was calculated with a second-order cumulant fit employing the standard Stokes−Einstein relation,

$$R_h = \frac{k_B T}{6\pi\eta D} \tag{19}$$

where k_B is Boltzmann's constant, T the absolute temperature, η the solvent's dynamic viscosity, and D the diffusion coefficient. The determined values of R_h are compared with the manufacturer's specifications in Table 1.

DLS and 2fFCS measurements were carried out at the same sample concentrations. Typical measurements and fit results of

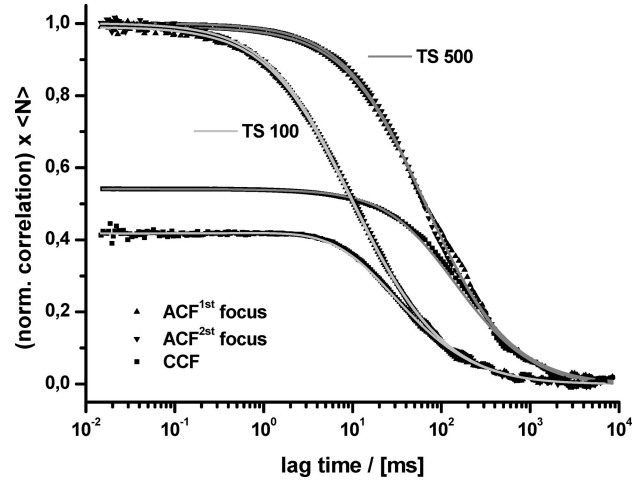

Figure 3. Typical 2fFCS measurement result for uniformly labeled latex beads of 50 nm (TS 100) and 250 nm (TS 500) radius. For comparison, correlation functions are normalized and multiplied by $\langle N \rangle$, which indicates the number of particles in the confocal volume. The autocorrelation function for the first focus (ACF^{1st} focus), second focus (ACF^{2nd} focus), and the cross correlation between both foci (CCF) are shown. Points indicate experimental values, and solid lines are global fits, using the extended model as described in the Theory section.

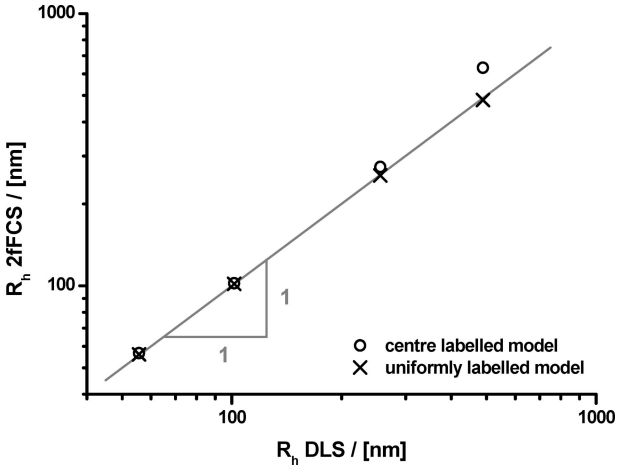

Figure 4. Comparison of DLS with 2fFCS for uniformly labeled latex beads. For 2fFCS, standard model and extended model were used for data analysis. Deviations of standard model from extended model results become significant for particle radii greater than ~200 nm.

TS 100 and TS 500 are exemplarily shown in Figure 3. Fitting was performed using the modified model as described in the Theory section, assuming a uniform labeling of particles. The effect of the decreasing amplitude ration of ACF to CCF, which is expected from the model, is more pronounced the larger the particles are and in good agreement with measured data.

A comparison between the results of DLS and our 2fFCS is shown in Figure 4. There, we show also the result of 2fFCS data analysis that assumes center labeling of particles (i.e., pointlike particles). As can be seen, the correspondence between DLS and extended model 2fFCS is excellent. Also, a clear difference between 2fFCS models assuming center and extended labeling can be seen. The deviation between standard model and extended model becomes significant for particle radius values above ~200 nm. In this case, radius values obtained with the standard model are distinctly larger than those obtained from DLS and extended model 2fFCS.

Recently FCS has been applied to study colloidal systems[17,27–34] where the aspect of fluorophor distribution inside the particle becomes relevant when the particle size increase. As single dye labeling on extended objects is rather difficult to archive, the models for different label geometries proposed in this paper provide a means to extend the applicability of FCS and 2fFCS in colloid and polymer science.

Conclusions

In this contribution, we considered the impact of non-negligible particle size with different fluorescent labeling on FCS and 2fFCS measurements. An extended model was developed for taking into account size and labeling effects in 2fFCS data analysis. Various labeling distributions and their influence on correlation functions were theoretically modeled and discussed. Next, we performed DLS and 2fFCS measurements on large uniformly labeled latex beads of different sizes. We found excellent agreement between DLS and 2fFCS measurements when applying our extended model to 2fFCS data analysis. The experimentally determined values for the hydrodynamic radius as calculated with the extended model were in perfect agreement with the specifications of the bead manufacturer as well as with the results from the DLS measurements. The proposed models for different labeling geometries allow utilization of 2fFCS (and also standard FCS) as a powerful complementary method to investigate extended objects in colloid and polymer science, e.g., refs 10–17. They offer the opportunity to use 2fFCS for absolute and precise measurement techniques of hydrodynamic radii of large diffusing objects at very low concentrations.

Acknowledgment. We are indebted to the whole team at PicoQuant Co. (Berlin, Germany). Financial support by the Deutsche Forschungsgemeinschaft (SPP1259) is gratefully acknowledged. J.E. thanks the Deutsche Volkswagenstiftung for its financial support.

References and Notes

(1) Einstein, A.; Fürth, R. *Investigations on the Theory of the Brownian Movement*; Dover: New York, 1956.
(2) Berne, B. J.; Pecora, R. *Dynamic Light Scattering: With Applications to Chemistry, Biology and Physics*; Wiley: New York, 1976.
(3) Callaghan, P. T. *Principles of Nuclear Magnetic Resonance Microscopy*; Clarendon Press/Oxford University Press: New York, 1991.
(4) Cole, J. L.; Hansen, J. C. *J. Biomol. Tech.* **1999**, *10*, 163.
(5) Magde, D.; Webb, W. W.; Elson, E. *Phys. Rev. Lett.* **1972**, *29*, 705.
(6) Elson, E. L.; Magde, D. *Biopolymers* **1974**, *13*, 1.
(7) Magde, D.; Elson, E. L.; Webb, W. W. *Biopolymers* **1974**, *13*, 29.
(8) Dertinger, T.; Pacheco, V.; von der Hocht, I.; Hartmann, R.; Gregor, I.; Enderlein, J. *ChemPhysChem* **2007**, *8*, 433.
(9) Starchev, K.; Zhang, J. W.; Buffle, J. *J. Colloid Interface Sci.* **1998**, *203*, 189.
(10) Caruso, F.; Donath, E.; Möhwald, H. *J. Phys. Chem. B* **1998**, *102*, 2011.
(11) Sukhorukov, G. B.; Donath, E.; Lichtenfeld, H.; Knippel, E.; Knippel, M.; Budde, A.; Möhwald, H. *Colloids Surf. A* **1998**, *137*, 253.
(12) Radtchenko, I. L.; Sukhorukov, G. B.; Möhwald, H. *Colloids Surf. A* **2002**, *202*, 127.
(13) Skirtach, A. G.; Javier, A. M.; Kreft, O.; Köhler, K.; Alberola, A. P.; Möhwald, H.; Parak, W. J.; Sukhorukov, G. B. *Angew. Chem. Int. Ed.* **2006**, *45*, 4612.
(14) Miksch, T.; Melzer, A. *Phys. Rev. E* **2007**, *75*, 016404.
(15) Zhang, R. J.; Cui, J. W.; Lu, D. M.; Hou, W. G. *Chem. Commun.* **2007**, *25*, 1547.
(16) Burkhardt, M.; Kasteel, R.; Vanderborght, J.; Vereecken, H. *Eur. J. Soil Sci.* **2008**, *59*, 82.
(17) Wong, J. E.; Müller, C. B.; Laschewsky, A.; Richtering, W. J. *Phys. Chem. B* **2007**, *111*, 8527.
(18) Böhmer, M.; Pampaloni, F.; Wahl, M.; Rahn, H. J.; Erdmann, R.; Enderlein, J. *Rev. Sci. Instrum.* **2001**, *72*, 4145.
(19) Müller, C. B.; Weiβ, K.; Richtering, W.; Loman, A.; Enderlein, J. *Opt. Express* **2008**, *16*, 4322.
(20) O'Connor, D. V.; Phillips, D. *Time Correlated Single Photon Counting*; Academic Press: London, 1984.
(21) Wahl, M.; Gregor, I.; Patting, M.; Enderlein, J. *Opt. Express* **2003**, *11*, 3583.
(22) Müller, B. K.; Zaychikov, E.; Bräuchle, C.; Lamb, D. C. *Biophys. J.* **2005**, *89*, 3508.
(23) Lamb, D. C.; Müller, B. K.; Bräuchle, C. *Curr. Pharm. Biotechnol.* **2005**, *6*, 405.
(24) Müller, C. B.; Richtering, W. Manuscript in preparation.
(25) Barton, G. *Elements of Green's Functions and Propagation Potentials, Diffusion, and Waves*; Clarendon Press: Oxford, 1989.
(26) Watson, G. N. *A Treatise on the Theory of Bessel Functions*; University Press: Cambridge, 1922.
(27) Winkler, R. G.; Keller, S.; Rädler, J. O. *Phys. Rev. E* **2006**, *73*, 041919.
(28) Lumma, D.; Keller, S.; Vilgis, T.; Rädler, J. O. *Phys. Rev. Lett.* **2003**, *90*, 218301.
(29) Bonne, T. B.; Papadakis, C. M.; Lüdtke, K.; Jordan, R. *Colloid Polym. Sci.* **2007**, *285*, 491.
(30) Zettl, H.; Zettl, U.; Krausch, G.; Enderlein, J.; Ballauff, M. *Phys. Rev. E* **2007**, *75*, 061804.
(31) Michelman-Ribeiro, A.; Horkay, F.; Nossal, R.; Boukari, H. *Biomacromolecules* **2007**, *8*, 1595.
(32) Guo, X.; Lu, T.; Huang, X. *Colloid Polym. Sci.* **2008**, *286*, 469.
(33) Nagao, D.; Yokoyama, M.; Saeki, S.; Kobayashi, Y.; Konno, M. *Colloid Polym. Sci.* **2008**, in press, DOI: 10.1007/s00396−008−1855−5.
(34) Cohen, S. M. **2008**, *Colloid Polym. Sci.*, in press, DOI: 10.1007/s00396−008−1861−7.

JP802280U